Characterisation of High Frequency Inductive Power Transfer Receivers Using Pattern Recognition on the Transmit Side Waveforms

Juan M. Arteaga, Lingxin Lan, Christopher H. Kwan, David C. Yates and Paul D. Mitcheson
Department of Electrical and Electronic Engineering
Imperial College London
j.arteaga-saenz15@imperial.ac.uk

***Abstract*—This paper demonstrates the characterisation of inductively coupled receivers for high frequency inductive power transfer (HF-IPT) systems using pattern recognition on the inverter waveforms at the transmit side. The impedance reflected by the candidate receivers to the transmit coil was estimated using a model programmed to associate the experimental drain-voltage waveforms of the inverter when it drives a receiver under test to those when driving known loads. The necessity of employing this technique is due to the difficulty of accurately measuring current and voltage across the coil given the parasitic effects of probing and the precise skewing required to measure an impedance, especially at high Q-factor. The proposed technique is convenient for characterising and comparing the impedance reflected by candidate receivers for a particular application where there is a choice to be made with respect to the rectifier topologies and semiconductor technologies. Experimental results, using a 13.56 MHz 100 W inductive power transfer system, were obtained for a full-wave Class D rectifier using silicon (Si) and silicon carbide (SiC) Schottky diodes, and two Class E rectifiers using SiC diodes.**

I. Introduction

High Frequency inductive power transfer (HF-IPT) is an alternative to wirelessly power electronic devices without necessarily using magnetically permeable materials, since at high frequencies, low inductance coils ($<5\,\mu\mathrm{H}$) allow achieving good link efficiencies at low coupling [1]–[6]. This is advantageous because air-core low inductance coils allow for wireless power to be employed in lightweight applications. For example, our previous work [7] showcases small batteryless drones being powered by a $13.56\,\mathrm{MHz}$ HF-IPT system while they hover at distances higher than one coil radius from the transmitter.

A HF-IPT system consists of various power conversion blocks, from which the fundamental parts are illustrated in Fig. 1: an inverter to generate a high frequency current to drive the transmit coil (i_p), an IPT-link with mutually coupled inductances where k is the coupling factor, and a rectifier to output a DC voltage from a high frequency induced electromotive force in the receive coil ($\mathcal{E}_\mathrm{s}$). The design and construction of the circuits that comprise HF-IPT systems can be challenging: the topologies employed usually rely on precise tuning, measurements of the magnetics are difficult [8], [9], and the switching devices SPICE models do not include information of some parasitics which are key for megahertz power electronics designs (e.g. [10], [11]).

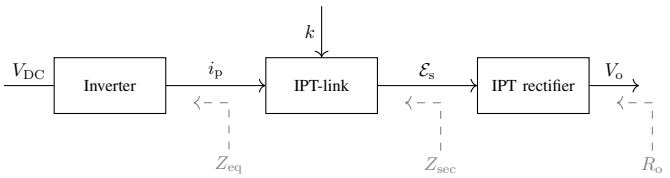

Fig. 1. HF-IPT system diagram.

One of the key variables which describes the interaction between the two ends of the system is the reflected impedance by the receiver to the transmit coil (Z_eq in Fig. 1). Knowledge of this variable in HF-IPT systems is typically limited to simulations since measuring it directly requires probing the current and the voltage across the transmit coil, which is difficult given the high current and voltage, the parasitics introduced by the probes, and the precise skewing required to calculate such impedance accurately.

In this work we implement an alternative to estimate Z_eq (introduced in our previous work [12]) where the variable to observe is the inverter transistor drain voltage (V_ds). V_ds is easier to measure since the inverter topology proposed (Class EF) has a capacitance across the switch. Also, this technique does not require information from any other probes, therefore eliminates skewing as a source of error. The principle of operation consists of observing the inverter waveforms at the transmit side as the DC load (R_o in Fig. 1) is stepped, and then comparing them to the waveforms when the inverter drives known loads.

This technique allows characterising inductively coupled receivers independent of the rectifier topology and semiconductor devices. Experiments were conducted on Class D and Class E rectifiers to compare Z_eq as R_o was stepped, and a comparison of a Class D rectifier using Si and SiC Schottky diodes was also conducted.

Copyright © 2020 IEEE. Personal use of this material is permitted. Permission from IEEE must be obtained for all other uses, in any current or future media, including reprinting/republishing this material for advertising or promotional purposes, creating new collective works, for resale or redistribution to servers or lists, or reuse of any copyrighted component of this work in other works by sending a request to pubs-permissions@ieee.org.
Citation: J. M. Arteaga, L. Lan, C. H. Kwan, D. C. Yates and P. D. Mitcheson, "Characterisation of High Frequency Inductive Power Transfer Receivers Using Pattern Recognition on the Transmit Side Waveforms," 2020 IEEE Applied Power Electronics Conference and Exposition (APEC), 2020, pp. 825-831. DOI: 10.1109/APEC39645.2020.9124398. IEEExplore link: https://ieeexplore.ieee.org/abstract/document/9124398

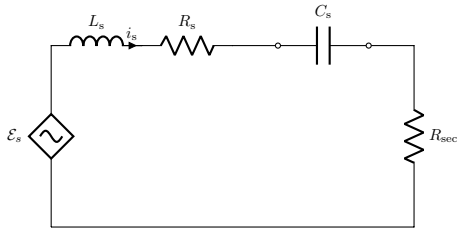

Fig. 2. Inductively coupled test-load circuit diagram.

II. Construction of an Experimental Impedance Estimation Tool

This section summarises the design and construction of the experimental-rig to estimate the reflected impedance of an inductively coupled receiver to a known transmitter. This tool was constructed based on our previous works [12], [13].

A. The Reflected Resistance and Reactance

The reflected impedance of an IPT receiver on the transmit coil (Z_{eq} in Fig. 1) is a fundamental parameter to design the inverter and the rectifier of a HF-IPT system: an inverter can be designed for a range of loads, and a rectifier can be designed to reflect a range of impedances. A first order approximation of Z_{eq} can be calculated as the sum of a reflected resistance and a reactance: $Z_{\mathrm{eq}} = R_{\mathrm{eq}} + jX_{\mathrm{eq}}$, where:

$$R_{\mathrm{eq}} = \frac{4\pi^2 f_{\mathrm{i_p}}^2 k^2 L_{\mathrm{p}} L_{\mathrm{s}} \left(R_{\mathrm{s}} + R_{\mathrm{sec}}\right)}{\left(R_{\mathrm{s}} + R_{\mathrm{sec}}\right)^2 + \left(2\pi f_{\mathrm{i_p}} L_{\mathrm{s}} + X_{\mathrm{sec}}\right)^2}, \tag{1}$$

$$X_{\mathrm{eq}} = -\frac{4\pi^2 f_{\mathrm{i_p}}^2 k^2 L_{\mathrm{p}} L_{\mathrm{s}} \left(2\pi f_{\mathrm{i_p}} L_{\mathrm{s}} + X_{\mathrm{sec}}\right)}{\left(R_{\mathrm{s}} + R_{\mathrm{sec}}\right)^2 + \left(2\pi f_{\mathrm{i_p}} L_{\mathrm{s}} + X_{\mathrm{sec}}\right)^2}, \tag{2}$$

k is coupling, $f_{\mathrm{i_p}}$ is the switching frequency, L_{p} and L_{s} are the self-inductances of the transmit and receive coils respectively, R_{p} and R_{s} are the equivalent series resistances of the transmit and receive coils respectively, R_{sec} is the input resistance of the rectifier and X_{sec} is the input reactance of the rectifier, including the series or parallel capacitance to resonate the receive coil. These equations can be derived from [1].

B. Design of a Test Load to Reflect a Known Impedance to the Transmitter

A test-load (Fig. 2), comprised of a receive coil (L_{s}, R_{s}), a capacitor (C_{s}) to resonate with L_{s} and a resistor (R_{sec}), was designed and built so that in an IPT setup where k is known, the reflected load can be calculated from (1) and (2). $\mathcal{E}_{\mathrm{s}}$ is the induced electromotive force on the receive coil.

To measure the reflected impedance of the test-load, the two terminals of the transmit coil which connect to the inverter were used as test points for a Keysight E4990A impedance analyser with a 42941A impedance probe to perform inductance and resistance measurements with respect to frequency. For these measurements, the inverter was disconnected from the coil. Fig. 3 shows the inductance (the sum of the self-inductance of the transmit coil and X_{eq} expressed as an inductance (L_{eq})) and resistance (the sum of the equivalent-series-resistance of the coil (R_{p}) and R_{eq}) measurement of the transmit coil inductively coupled to the test-load. It should be noted that this technique is not useful if the receiver has a rectifier since a large signal is required to activate the diodes, and also the junction capacitance of the diodes depends of the output voltage.

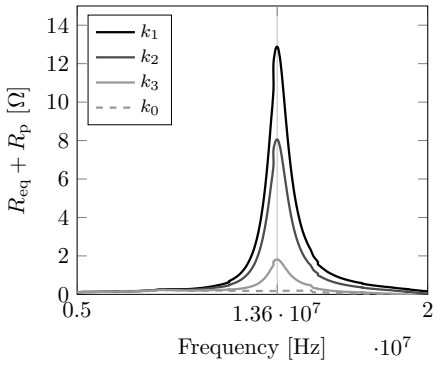

(a) Resistance

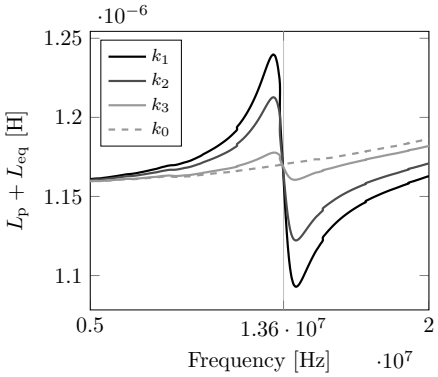

(b) Reactance

Fig. 3. Inductance and resistance measurement of a test coil coupled to the test-load using a E4990A Impedance Analyser by Keysight.

Here, as can be derived from (1) and (2), the maximum R_{eq}, and the point of convergence of the inductance measurements ($X_{\mathrm{eq}} = 0$), determine the frequency at which the test-load is tuned. This measurement allows not only for the test-load to be tuned accurately at the frequency of operation, but to detune it by changing C_{s} (Fig. 2) and allow for a X_{eq} different than zero.

C. Estimating the Reflected Impedance Using Class EF Inverters

Class EF inverters, extensively discussed in literature [14]–[17], can be designed to deal with changes in the load by designing the passive components shown in the circuit diagram (Fig. 5).

The effects produced by changes in the load resistance are well documented. For example, with the load-independent de-

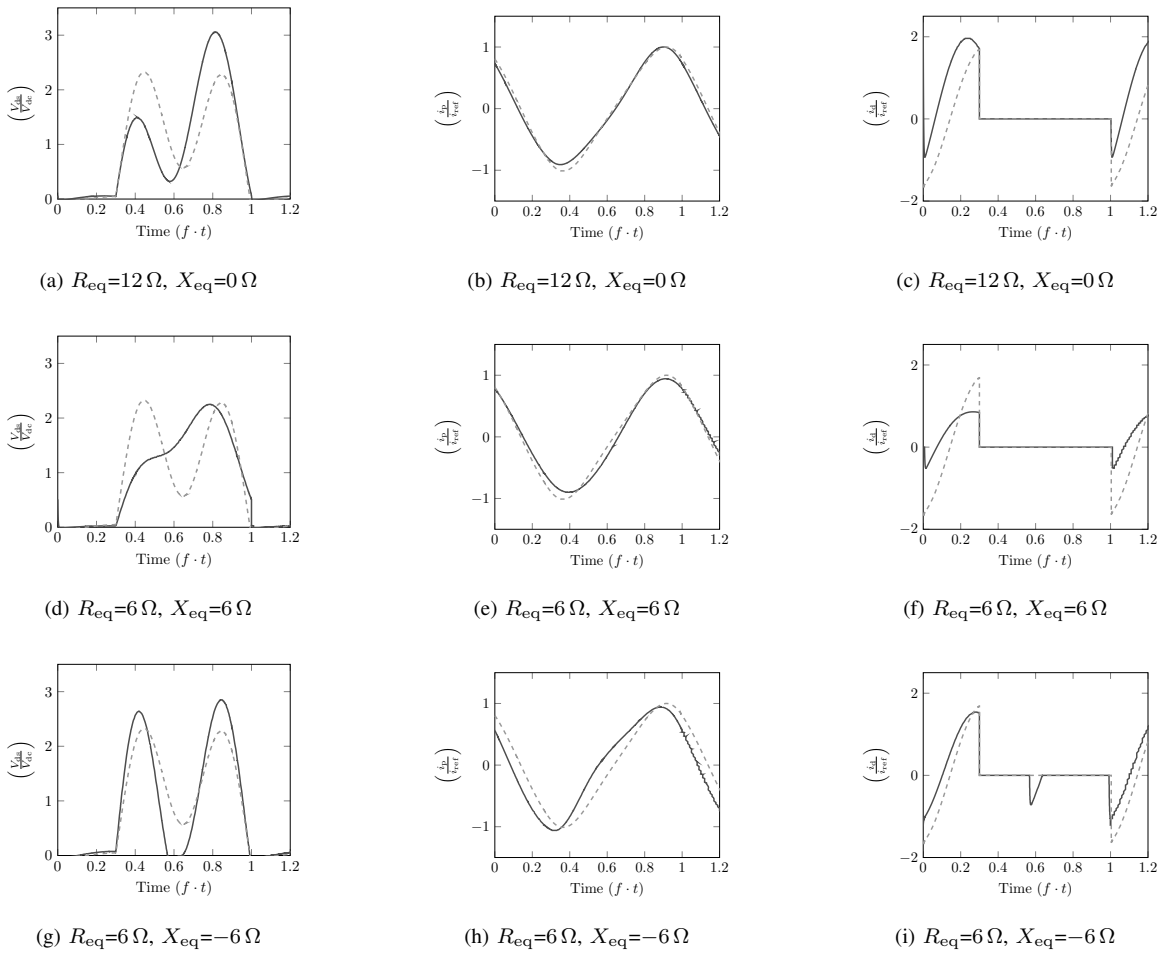

(a) R_{eq}=12 Ω, X_{eq}=0 Ω (b) R_{eq}=12 Ω, X_{eq}=0 Ω (c) R_{eq}=12 Ω, X_{eq}=0 Ω

(d) R_{eq}=6 Ω, X_{eq}=6 Ω (e) R_{eq}=6 Ω, X_{eq}=6 Ω (f) R_{eq}=6 Ω, X_{eq}=6 Ω

(g) R_{eq}=6 Ω, X_{eq}=−6 Ω (h) R_{eq}=6 Ω, X_{eq}=−6 Ω (i) R_{eq}=6 Ω, X_{eq}=−6 Ω

Fig. 4. Theoretical waveforms of a Load Independent Class EF inverter driving resistive, inductive-resistive and capacitive-resistive loads. The waveforms of the inverter when its not coupled to a receiver are marked as a dashed line.

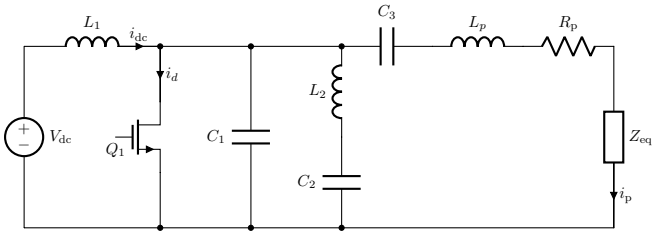

Fig. 5. Class EF inverter circuit diagram.

sign [17], which typical waveforms are shown in Fig. 4 (a,b,c), zero voltage switching is achieved independent of the load, and also the current amplitude and phase at which the transmit coil is driven do not change with load resistance. However, changes on X_{eq}, which effectively emulate changes on L_{p} (Fig. 3), can drastically affect the tuning. The theoretical waveforms in such cases are illustrated in Fig. 4 (d-i).

From the theoretical waveforms in Fig. 4, a clear difference in the shape of V_{ds} is observed once Z_{eq} changes in magnitude and phase, and since V_{ds} is relatively easy to measure (as opposed to for example i_{d}) it is well suited as the parameter to evaluate as the reflected impedance by a candidate receiver changes.

TABLE I
MEASUREMENTS OF THE COILS AT 13.56 MHz

Description	L_{p} and L_{s} [nH]	R_{p} and R_{s} [mΩ]	Q factor
Measurement	1181.0	202.7	496

A detailed description of the design of the inverter can be found in our previous work [5].

D. Construction of the HF-IPT System

A 13.56 MHz IPT test-rig was designed and built as proposed in [13]. It uses a load-independent Class EF inverter, two equal two-turn printed circuit board coils of 20 cm in outer diameter and a rectifier under test. The coils inductance and equivalent series resistance are shown in Table I. The coils were aligned with an air-gap of 14.7 cm. A WT310 Digital Power Meter by Yokogawa was used to measure the

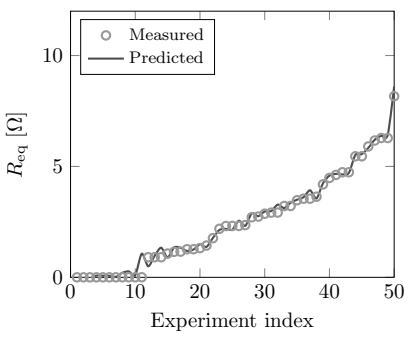

(a) Reflected resistance

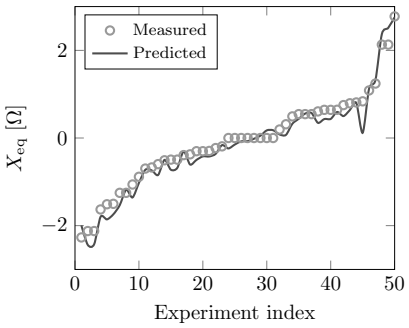

(b) Reflected reactance

Fig. 6. Impedance estimation model accuracy [12].

input power and a WT210 Digital Power Meter by Yokogawa was used to measure the output power. A Teledyne LeCroy HDO4054 oscilloscope with a 100:1 high voltage probe by PMK was used to measure V_{ds}.

E. Training a Model for Reflected Impedance Estimation

The inverter drain voltage waveforms were captured at ten different couplings using six different tunings of the test-load (different C_{s} in Fig. 2). The recorded waveforms were then used to train an impedance estimation model using a convolutional neural-network algorithm. The model accuracy was verified by using a portion of the data which was not used in the training process. The accuracy of this model was calculated with a coefficient of determination of 0.9899 for the real part and 0.9743 for the imaginary part. The prediction results are shown in Fig. 6.

III. Experimental HF-IPT Receiver Characterisation

The impedance estimation test-rig developed in the previous section was used to calculate Z_{eq} with respect to the DC-load (R_{o} in Fig. 1) for the candidate receivers. Firstly, Z_{eq} was compared using two different semiconductor technologies on a Class D rectifier, and secondly, two Class E rectifier designs were compared against the results obtained from the experiments with the Class D rectifier.

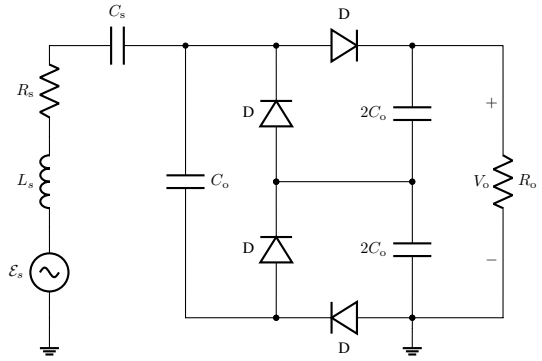

Fig. 7. Voltage-doubler Class D rectifier.

A. The Reflected Impedance of a HF-IPT Receiver With a Class D Rectifier

A current-driven voltage-doubler Class D rectifier (Fig. 7) was designed, built and tuned to the receive coil of the proposed HF-IPT system. This rectifier was built using an in-house rectifier evaluation board for diodes with TO-252 package. C_{s} was designed to resonate the self-inductance of the receive coil and the output capacitor C_{o} was designed to be $1\,\mu\mathrm{F}$. The diodes under test are: STPSC8H065-Y by STMicroelectronics (SiC Schottky) and: MBRD10200CT by Littelfuse (Si Schottky).

The results of the measurement of Z_{eq} as function of R_{o} are shown in Fig. 8. The plots show that the behaviour of the built rectifiers is different to that of the rectifier with ideal diodes. A HF-IPT receiver with a Class D rectifier is expected to reflect a constant reactance (zero if the receiver is tuned) but as can be seen from the plots in Fig. 8 (b) X_{eq} changes with load, hence behaving like a Class DE rectifier. Once the models of the real components are integrated in the SPICE simulation, a variation in X_{eq} can be accounted for, however the variation in X_{eq} measured in the experiments is significantly higher than that expected from simulation.

Interestingly, in the experiments with the rectifier that uses SiC Schottky diodes, a higher peak R_{eq} is reached when compared to the R_{eq} peak of the experiments with the rectifier that uses Si Schottky diodes. This measurement coincides with the power measurements shown in Fig. 9 in that the system input power (P_{i}) peaks at the same value of R_{o} as R_{eq}, and that the highest peak in P_{i} of the rectifier with SiC Schottky diodes is higher than the one with Si Schottky diodes. However, the peak output power (P_{o}) is roughly the same for both rectifiers. The rectifier with SiC Schottky diodes fails to achieve a higher output power than the Si alternative despite reflecting a higher R_{eq} to the transmitter. Since both P_{i} and R_{eq} are higher, but not P_{o}, and since the only alteration in the experiments is the diodes of the rectifier, the experiments strongly suggest that the rectifier with SiC Schottky diodes has higher losses in its devices. This is to an extent expected since the forward voltage of the SiC Schottky diodes is higher than that of the Si Schottky diodes, therefore as R_{o} decreases, and consequently

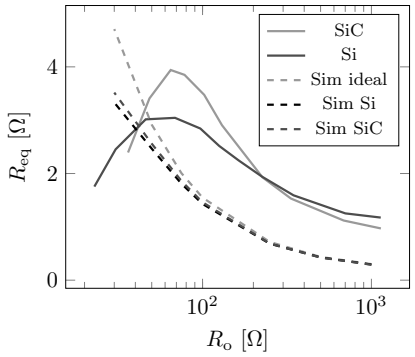

(a) Reflected resistance

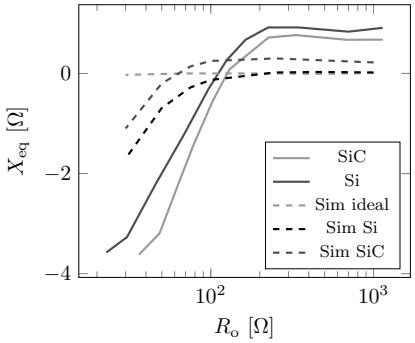

(b) Reflected reactance

Fig. 8. Measured and simulated Z_{eq} with the Class D rectifier employing Si Schottky and SiC Schottky diodes. Sim refers to results from a SPICE simulation.

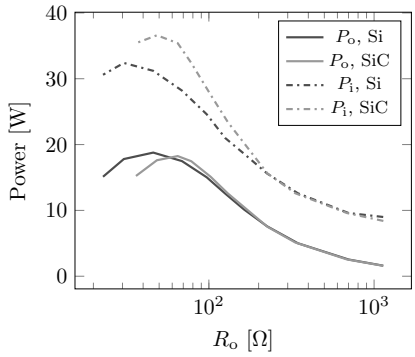

(a) Input and output power

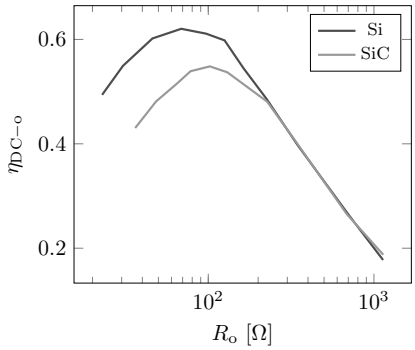

(b) End-to-end efficiency

Fig. 9. DC power measurements and DC input to DC output efficiency of the Class D rectifiers.

the output current increases, the conduction losses in the SiC diodes become more significant in the overall efficiency.

B. The Reflected Impedance of a HF-IPT Receiver With a Class E Rectifier

An alternative topology for HF-IPT rectifiers is the Class E. Diode Class E rectifiers have an input reactance that changes with load, even with ideal diodes, but since there is a capacitance in parallel with the diode in the topology, the diode junction capacitance can be accounted for in the design. Therefore, the rectifier can be designed more accurately since this parasitic capacitance does not change the topology of the rectifier, as does the Class D, behaving like a Class DE. The work in [18] demonstrated various tuning techniques for Class E rectifiers in HF-IPT environments. A hybrid Class E rectifier is proposed to minimise the X_{eq} dependence of load, and a set of designs are proposed to achieve this. Two full-wave hybrid Class E rectifiers (the topology is shown in Fig. 10) were designed and built as proposed in [18] to evaluate this criteria. Table II shows the components of the built prototypes. The diodes used are 650 V, 30 A SiC Schottky diodes by Cree (C3D10065A).

The Z_{eq} plots with respect to R_{o} are shown in Fig. 11. A significant lower variation in X_{eq} can be seen with respect to

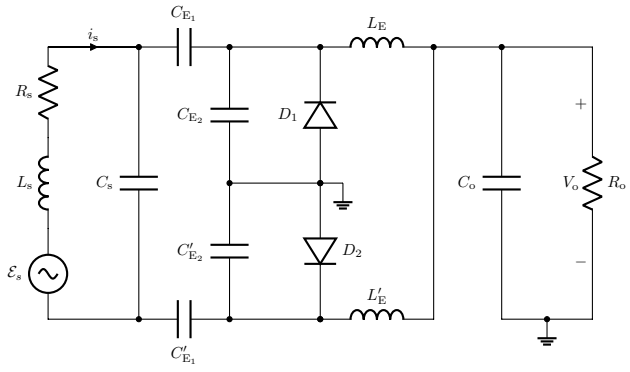

Fig. 10. Full-wave hybrid Class E rectifier.

TABLE II
COMPONENT VALUES OF THE RECTIFIERS: PUSH-PULL HYBRID CLASS E

Design	L_{E} [nH]	C_s [pF]	$C_{\mathrm{E_1}}$ [pF]	$C_{\mathrm{E_2}}$ [pF]	C_o [µF]
$\mathrm{E_1}$	270	36	110	64	1
$\mathrm{E_2}$	800	24	186	30	1

the Class D rectifiers. Therefore, surprisingly, for roughly the same power range of 0 W to 20 W (Fig. 12), the Class E

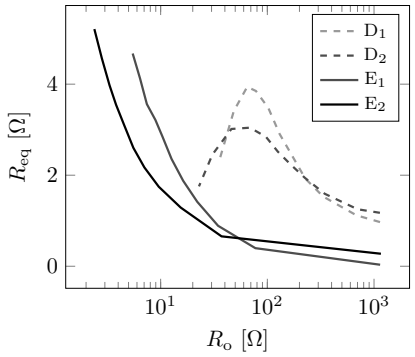

(a) Reflected resistance

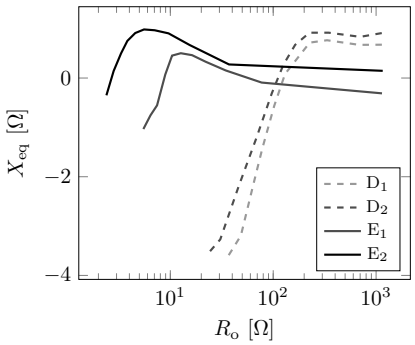

(b) Reflected reactance

Fig. 11. Measured Z_{eq} with the Class E rectifier. The measured Class D rectifiers Z_{eq} are plotted with dashed lines.

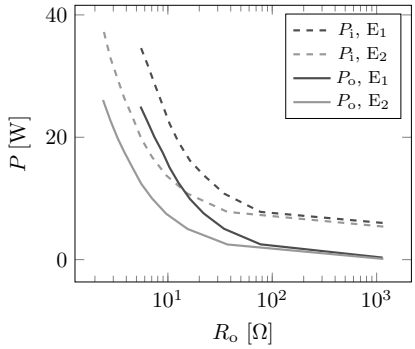

(a) Input and output power

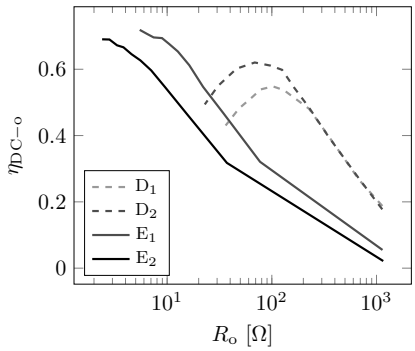

(b) end-to-end efficiency

Fig. 12. DC power measurements and DC input to DC output efficiency of the system with Class E rectifiers.

alternative has a lower X_{eq} variation than the Class D, notwithstanding that the latter, in principle, should have zero variation in X_{eq}.

The Class E prototypes use SiC Schottky diodes, and despite operating at lower R_{o}, and therefore at higher output current than the Class D prototypes, they achieve a higher end-to-end efficiency.

IV. Conclusion

An in-house HF-IPT reflected impedance estimation test-rig was implemented to characterise the impedance reflected by four HF-IPT receivers under test which employ different rectifiers. This test-rig allows calculating the reflected impedance by observing and comparing the inverter waveforms once the candidate receivers are coupled to the transmit coil.

In the experiments we demonstrate that the reflected impedance of a HF-IPT receiver with a Class D rectifier is not solely resistive, and that the reactance variation is similar if the rectifier is constructed with SiC or Si Schottky diodes, however in this topology, the SiC diodes can introduce additional losses once the load resistance is low due to higher conduction losses.

The lowest reflected reactance variation was achieved with the hybrid Class E rectifiers, which allow tuning for this feature. Given that this topology has only two diodes (the full-wave version), as opposed to four of the Class D, and that since the reflected reactance is lower, thus minimising the detuning of the inverter, a higher efficiency was also achieved with this topology.

Acknowledgement

The authors would like to acknowledge Dr. George Kkelis for the design of the Class E rectifiers, and the following funding sources: Department of Electrical and Electronic Engineering, Imperial College London; PINN Programme, Ministry of Science and ICT of Costa Rica MICITT; University of Costa Rica; EPSRC Converter Architectures, grant ref: EP/R004137/1.

References

[1] K. Van Schuylenbergh and R. Puers, *Inductive powering: Basic theory and application to biomedical systems*. Springer Science & Business Media, 2009.

[2] A. Kurs, A. Karalis, R. Moffatt, J. D. Joannopoulos, P. Fisher, and M. Soljačić, "Wireless power transfer via strongly coupled magnetic resonances," *science*, vol. 317, no. 5834, pp. 83–86, 2007.

[3] S. Y. R. Hui, W. Zhong, and C. K. Lee, "A critical review of recent progress in mid-range wireless power transfer," *IEEE Trans. on Power Electron.*, vol. 29, no. 9, pp. 4500–4511, Sept 2014.

[4] M. Pinuela, D. C. Yates, S. Lucyszyn, and P. D. Mitcheson, "Maximizing DC-to-load efficiency for inductive power transfer," *IEEE Trans. on Power Electron.*, vol. 28, no. 5, pp. 2437–2447, May 2013.

[5] J. M. Arteaga, S. Aldhaher, G. Kkelis, D. C. Yates, and P. D. Mitcheson, "Multi-MHz IPT systems for variable coupling," *IEEE Trans. on Power Electron.*, vol. 33, no. 9, pp. 7744–7758, Sept 2018.

[6] G. Zulauf and J. M. Rivas Davila, "Single-turn air-core coils for high-frequency inductive wireless power transfer," *IEEE Trans. on Power Electron.*, pp. 1–1, 2019.

[7] J. M. Arteaga, S. Aldhaher, G. Kkelis, C. Kwan, D. C. Yates, and P. D. Mitcheson, "Dynamic capabilities of multi-MHz inductive power transfer systems demonstrated with batteryless drones," *IEEE Trans. on Power Electron.*, vol. 34, no. 6, pp. 5093–5104, June 2019.

[8] W. B. Kuhn and A. P. Boutz, "Measuring and reporting high quality factors of inductors using vector network analyzers," *IEEE Trans. Microw. Theory Techn.*, vol. 58, no. 4, pp. 1046–1055, 2010.

[9] J. Lawson, D. C. Yates, and P. D. Mitcheson, "High Q coil measurement for inductive power transfer," *IEEE Trans. Microw. Theory Techn.*, pp. 1–12, 2019.

[10] G. D. Zulauf, J. Roig-Guitart, J. D. Plummer, and J. M. Rivas-Davila, "C_{OSS} measurements for superjunction mosfets: Limitations and opportunities," *IEEE Trans. Electron Devices*, vol. 66, no. 1, pp. 578–584, 2018.

[11] Z. Tong, G. Zulauf, J. Xu, J. D. Plummer, and J. Rivas-Davila, "Output capacitance loss characterization of silicon carbide schottky diodes," *IEEE Trans. Emerg. Sel. Topics Power Electron.*, vol. 7, no. 2, pp. 865–878, 2019.

[12] L. Lan, J. M. Arteaga, D. C. Yates, and P. D. Mitcheson, "A reflected impedance estimation technique for inductive power transfer," in *IEEE PELS Workshop on Emerging Technologies: Wireless Power (WoW)*, June 2019, pp. 1–4.

[13] J. M. Arteaga, L. Lan, S. Aldhaher, G. Kkelis, D. C. Yates, and P. D. Mitcheson, "A multi-MHz IPT-link developed for load characterisation at highly variable coupling factor," in *IEEE Wireless Power Transfer Conf. (WPTC)*, June 2018, pp. 1–4.

[14] Z. Kaczmarczyk, "High-efficiency Class E, EF_2 , and E/F_3 inverters," *IEEE Trans. on Ind. Electron.*, vol. 53, no. 5, pp. 1584–1593, Oct 2006.

[15] R. C. N. Pilawa-Podgurski, A. D. Sagneri, J. M. Rivas, D. I. Anderson, and D. J. Perreault, "Very-high-frequency resonant boost converters," *IEEE Trans. on Power Electron.*, vol. 24, no. 6, pp. 1654–1665, June 2009.

[16] S. Aldhaher, D. C. Yates, and P. D. Mitcheson, "Modeling and analysis of Class EF and Class E/F inverters with series-tuned resonant networks," *IEEE Trans. on Power Electron.*, vol. 31, no. 5, pp. 3415–3430, May 2016.

[17] ——, "Load-independent class E/EF inverters and rectifiers for MHz-switching applications," *IEEE Trans. on Power Electron.*, pp. 1–1, 2018.

[18] G. Kkelis, D. C. Yates, and P. D. Mitcheson, "Class-E half-wave zero dv/dt rectifiers for inductive power transfer," *IEEE Trans. on Power Electron.*, vol. 32, no. 11, pp. 8322–8337, Nov 2017.